© 2018. This manuscript version is made available under the CC-BY-NC-ND 4.0 license
http://creativecommons.org/licenses/by-nc-nd/4.0/
Post-Print Version
https://doi.org/10.1016/j.brs.2018.04.011

Atlas of Optimal Coil Orientation and Position for TMS: A Computational Study

Jose Gomez-Tames[a], Atsushi Hamasaka[a], Ilkka Laakso[b],

Akimasa Hirata[a], Yoshikazu Ugawa[c,d]

a. Nagoya Institute of Technology, Department of Electrical and Mechanical Engineering, Nagoya, Aichi 466-8555, Japan

b. Aalto University, Department of Electrical Engineering and Automation, Espoo FI-00076, Finland

c. Fukushima Medical University, Department of Neurology, School of Medicine, Fukushima, 960-1295, Japan

d. Aizu Chuo Hospital, Department of Neurology, Aizuwakamatsu city, Fukushima, 965-8611, Japan

*Corresponding Authors:
Jose Gomez-Tames* and Akimasa Hirata**
Tel & Fax: +81-52-735-7916
*E-mail:jgomez@nitech.ac.jp
** E-mail:ahirata@nitech.ac.jp

This is an author-created, un-copyedited version of an article published in Brain Stimulation. The Version of Record is available online at https://doi.org/10.1016/j.brs.2018.04.011

© 2018. This manuscript version is made available under the CC-BY-NC-ND 4.0 license
http://creativecommons.org/licenses/by-nc-nd/4.0/
Post-Print Version
https://doi.org/10.1016/j.brs.2018.04.011

Abstract

Background: Transcranial magnetic stimulation (TMS) activates target brain structures in a non-invasive manner. The optimal orientation of the TMS coil for the motor cortex is well known and can be estimated using motor evoked potentials. However, there are no easily measurable responses for activation of other cortical areas and the optimal orientation for these areas is currently unknown.

Objective: This study investigated the electric field strength, optimal coil orientation, and relative locations to optimally stimulate the target cortex based on computed electric field distributions.

Methods: A total of 518,616 stimulation scenarios were studied using realistic head models (2401 coil locations × 12 coil angles × 18 head models). Inter-subject registration methods were used to generate an atlas of optimized TMS coil orientations on locations on the standard brain.

Results: We found that the maximum electric field strength is greater in primary somatosensory cortex and primary motor cortex than in other cortical areas. Additionally, a universal optimal coil orientation applicable to most subjects is more feasible at the primary somatosensory cortex and primary motor cortex. We confirmed that optimal coil angle follows the anatomical shape of the hand motor area to realize personalized optimization of TMS. Finally, on average, the optimal coil positions for TMS on the scalp deviated 5.5 mm from the scalp points with minimum cortex-scalp distance. This deviation was minimal at the premotor cortex and primary motor cortex.

Conclusion: Personalized optimal coil orientation is preferable for obtaining the most effective stimulation.

Keywords: Transcranial Magnetic Stimulation; Optimization of Coil Orientation, Brain Atlas, Personalized Stimulation

© 2018. This manuscript version is made available under the CC-BY-NC-ND 4.0 license
http://creativecommons.org/licenses/by-nc-nd/4.0/
Post-Print Version
https://doi.org/10.1016/j.brs.2018.04.011

Introduction

Transcranial magnetic stimulation (TMS) induces an eddy current in the brain to activate a target area when a strong pulsed current is injected into a coil (1). Recent studies report that the nature of various complicated brain structures results in non-uniform current distribution in a brain when stimulated by TMS (2–7). How to efficiently stimulate target cortical areas of varied structures remains unclear. The main physical agent known to activate neurons is the electric field (or the current density), although its relative direction to the neural structures is also important, from a microscopic viewpoint. Dominant factors affecting the electric field are the coil orientation and position, relative to the gyri and sulci of the brain (8). The optimal coil orientation is well-known for the motor cortex (9–11), owing to the presence of a relatively straightforward measurable marker of activation for each individual subject, such as the threshold for motor evoked potentials (MEPs) and their amplitudes or latencies (12). Computational studies have also shown that the coil orientation inducing posterior-anterior directed currents in the hand motor area resulted in the highest electric fields in this region (13). However, the most effective coil configuration remains to be determined for other areas due to a lack of proper measurable biomarkers. We have no ways to estimate either the size of the electric field required for those areas as compared with the motor cortex, or the optimal orientation and position of the coil. These factors likely depend on the individual differences in neuroanatomy, but these factors have not been studied yet.

We investigated the electric field strength and optimal coil orientation in a group of healthy subjects to find (a) systematic differences in electric field strengths between different brain regions, (b) universally optimal coil direction (if present) for each brain region, and (c) how far the optimal coil position deviates from the scalp point nearest to the target cortical area. The results presented here can be used as a guide for selecting TMS intensity and angle when stimulating non-motor cortical areas.

© 2018. This manuscript version is made available under the CC-BY-NC-ND 4.0 license
http://creativecommons.org/licenses/by-nc-nd/4.0/
Post-Print Version
https://doi.org/10.1016/j.brs.2018.04.011

Materials and methods

Head Models

The head models of eighteen subjects were constructed from T1- and T2-weighted images (available on: http://hdl.handle.net/1926/1687) and represented by a grid of cubical voxels (4×10^6 voxels with a resolution of 0.5 mm). The mean age of the sample population was 43.4 ± 9.8 years (all subjects are male and neurologically healthy). The models were segmented into 14 tissues/body fluids (skin, fat, muscle, outer skull, inner skull, grey matter, white matter, cerebellar grey matter, cerebellar white matter, brainstem, nuclei, ventricles, cerebrospinal fluid, and eyes) as shown in Fig. 1. In brief, the FreeSurfer image analysis software (14,15) was used to reconstruct the surfaces of the grey and white matter. Non-brain tissues were segmented from T1- and T2-weighted Magnetic Resonance Images (MRIs) with a semi-automatic procedure using the region-growing and thresholding techniques as described previously (16). Note that the cerebrospinal fluid was the volume inside the skull that was not classified as nervous tissue or blood explicitly.

A spherical model was also implemented to represent the head. Its effective radius (91 to 97 mm) was derived from the eighteen realistic head models such that the sphere fits the scalp surface.

Computer Simulation

A volume conductor model was used to compute induced electric fields in head models. We assumed that the electric displacement current is negligible when compared to the conduction current (magneto-quasi-static approximation), and induced current does not perturb the external magnetic field. The induced scalar potential ϕ is given by:

$$\nabla \cdot [\sigma(-\nabla \phi - j\omega \mathbf{A}_0] = 0, \quad \text{(Eq.1)}$$

where $\mathbf{A}_0$ and σ denote the magnetic vector potential of the applied magnetic field and tissue conductivity, respectively.

© 2018. This manuscript version is made available under the CC-BY-NC-ND 4.0 license
http://creativecommons.org/licenses/by-nc-nd/4.0/
Post-Print Version
https://doi.org/10.1016/j.brs.2018.04.011

The electric conductivity of head tissues was assumed to be linear and isotropic. Two sets of conductivities were used, as shown in Table 1. The tissue conductivities of set A were determined using the fourth order Cole-Cole model (17) at 10 kHz (18), whereas the values used in set B corresponded to typical values in other TMS computational models (19–21). Set A was used throughout all the computations, and set B was used in the subsection "Uncertainty factors" in Results. The electric field was calculated at a depth of 0.8 mm below the grey matter surface to mitigate the risk of numerical artifacts of the surface voxels.

A figure-8 magnetic stimulation coil with a wing outer diameter of 9.7 cm and an inner diameter of 4.7 cm was modeled using the thin-wire approximation, and the magnetic vector potential was calculated using the Biot–Savart law. The coil current was fixed to 1 A for all simulations. The electric fields induced in the head model were determined from the vector potential using the finite-element method with first-order cubical elements (22).

Stimulation Scenarios

The coil plane was normal to the stimulation point on the surface of the scalp. A distance of 6 mm was maintained between the center of the figure-8 coil, where the two loops meet, and the scalp point. We used a normal vector that was averaged over a round area around the stimulation point (5 cm of radius) and thus, eliminating the effect of small bumps of the scalp surface. The angle = 0 ˚ (vertical axis) corresponded to a line in the coil plane normal to the longitudinal fissure (i.e., the medial border of the coil plane is parallel to the longitudinal fissure), as shown in Fig. 2B. The coil was only rotated around its vertical axis and fixed on its lateral and longitudinal axes. The fixed angle in lateral and longitudinal axes was defined when the coil was normal to the scalp at the vertical axis of rotation of 0° for each stimulation point.

In each head model, 28,812 stimulation scenarios [s] were investigated. They corresponded to a magnetic coil placed over 2,401 locations (grid of approximately 5-mm resolution in Fig. 2A) at 12 different coil orientations (15-degree interval). The total number of simulations was 518,616 across all the subjects.

© 2018. This manuscript version is made available under the CC-BY-NC-ND 4.0 license
http://creativecommons.org/licenses/by-nc-nd/4.0/
Post-Print Version
https://doi.org/10.1016/j.brs.2018.04.011

Individual Cortical Maps

In each subject, we stored the maximum electric field among [s] (combination of j coil rotations and k stimulation points) for each voxel i in the brain tissue. Further, the optimal coil orientation $\alpha_{\mathrm{opt}}(i)$ and optimal location $\mathbf{L}_{\mathrm{opt}}(i)$ corresponding to the maximum electric field in each point of the cortical surface, were stored. They were calculated from the following formulae:

$$E_{\mathrm{max}}(i) = max_{\mathrm{j}\times\mathrm{k}\in[s]} \left|\mathbf{E}(\alpha_{\mathrm{j}}(i), \mathrm{L_k}(i))\right|, \text{(Eq.2)}$$

$$(\alpha_{\mathrm{opt}}(i), \mathbf{L}_{\mathrm{opt}}(i)) = argmax_{j\times k\in[s]} \left|\mathbf{E}(\alpha_{\mathrm{j}}(i), \mathrm{L_k}(i))\right|. \text{(Eq.3)}$$

To determine how far the optimal coil position for TMS on the scalp deviates from the scalp point nearest to the cortical surface $\mathbf{L}_{\mathrm{near}}$ (minimum cortex-scalp distance), $\mathbf{L}_{\mathrm{shift}}$ was calculated as the Euclidean distance between both locations

$$L_{\mathrm{shift}}(i) = \left|\mathbf{L}_{\mathrm{opt}}(i) - \mathbf{L}_{\mathrm{near}}(i)\right| . \text{(Eq.4)}$$

For each subject, E_{max} (Fig. 3-B1 to Fig. 3-S2), α_{opt} (Fig. 5-B1 to Fig. 5-S2), and L_{shift} of the original cortical surface were registered to a common standard brain space. The registration procedure was similar to that in our previous studies (16) and is described below.

The optimal coil angle in the motor area and the normal vector to the cortical surface were computed to determine if the optimal coil orientation follows the motor cortical anatomy (Fig. 6C). To target the motor area, the coil was positioned at 480 scalp points and rotated with steps of 5˚, as shown in Fig. 6A. We selected points along the gyral crown and corresponding wall points (i.e., middle depth) to find the correlation between the computed optimal angles (Fig. 6-B1) and the angle normal to the sulcus wall (Fig. 6-B2) in six subjects. A weighted mean Fisher z-transformed correlation coefficient value was calculated and transformed back to correlation coefficients using the inverse of the Fisher z transformation (23).

© 2018. This manuscript version is made available under the CC-BY-NC-ND 4.0 license
http://creativecommons.org/licenses/by-nc-nd/4.0/
Post-Print Version
https://doi.org/10.1016/j.brs.2018.04.011

Universal Cortical Maps

In order to minimize inter-individual effects, we combined all the subjects' maps. The $\overline{E}_{\max}$ and $\bar{L}_{\text{shift}}$ maps (Fig. 3-A1 and Fig. 7) were the averages of $E_{\max}$ and L_{shift} in the standard brain space across all the subjects after normalization. The inter-individual effect was quantified by the relative standard deviation of $E_{\max}$ and L_{shift} maps across all subjects.

The set $\alpha_{90\%}(i)$ was composed of the non-repeated coil angles that induce field strength larger than $0.9E_{\max}(i)$ in each subject. The optimum coil orientation map $\bar{\alpha}_{\text{opt}}$ was the mode of the set $\alpha_{90\%}$ across all subjects (Fig. 5-A1). The inter-individual effect was quantified as the percentage of subjects that present the optimal coil angle in $\bar{\alpha}_{\text{opt}}$ map (Fig. 5-A2).

Statistical comparisons of $\overline{E}_{\max}$ values were performed between the following cortical regions: precentral and postcentral gyri, as well as frontal, parietal, occipital, and temporal lobes. The statistical comparisons were also performed for $\bar{L}_{\text{shift}}$ and percentage of subjects with common optimal angle maps. One-way ANOVA followed by a Bonferroni-corrected post-hoc t-tests were used to assess differences.

Registration Method

The procedure to register the electric field and TMS orientation for each subject on the standard brain template was similar to that used previously (16). Cortical surface reconstructions were registered by FreeSurfer on the default FreeSurfer brain template (FS40). Next, the cortical surface representation of the MNI ICBM 2009a standard brain (24,25) were registered using the same FS40 template. Surface-to-surface registration was used. Combining the first registration and the inverse of the second, we obtained a map of the anatomical area of each individual brain with respect to the corresponding anatomical area in the MNI standard brain template.

© 2018. This manuscript version is made available under the CC-BY-NC-ND 4.0 license
http://creativecommons.org/licenses/by-nc-nd/4.0/
Post-Print Version
https://doi.org/10.1016/j.brs.2018.04.011

Results

Electric Field Distribution for Optimal Orientation and Coil Position

Fig. 3 shows the maximum electric field that can be achieved in all the cortical areas for an optimum coil orientation and scalp position. Fig. 3-A1 shows the sites where the maximum electric field consistently appears despite subject-specific variations. In most cases, the electric field in the gyri was stronger than in the sulci and almost uniform (red regions), such as in the primary somatosensory cortex, primary motor cortex, and Broca's area. Likewise, Fig. 3-A2 shows the standard deviation of induced currents on each stimulation site, whose comparison with figure A1 reveals that areas with lower inter-subject variability corresponded to areas with larger electric field induction.

The averaged cortex-scalp distance had a similar spatial distribution to that of the averaged electric field strength ($R^2 = 0.7985$, $p < 0.001$), as shown in Fig. 4A. Also, the root-mean-square error between the electric field strength and the cortex-scalp distance of all subjects at each cortical point is presented in Fig. 4B. Fig. 4C depicts the variation of the maximum electric field at different distances from the scalp; the electric field strength decays with distance from the scalp (approximately cubic). The results are also consistent with those of a spherical model with a diameter of 8.5 cm (26).

Optimal Coil Orientation

As shown in Fig. 5B–5S, the optimal coil orientation inducing the maximum electric field depends on the target brain area. Fig. 5-A1 shows the most common optimal coil orientation that can induce an electric field strength larger than 90% of the maximum value in the maximum number of subjects. This $\bar{\alpha}_{\mathrm{opt}}$ map confirms the expected coil orientation to the gyrus. Specifically, the optimal induced current direction has been shown to be close to being perpendicular to the gyrus (10,27–29) in the hand motor area, with which our findings generally agree. Fig. 5-A2 presents the maximum percentage of subjects with a common optimal angle.

© 2018. This manuscript version is made available under the CC-BY-NC-ND 4.0 license
http://creativecommons.org/licenses/by-nc-nd/4.0/
Post-Print Version
https://doi.org/10.1016/j.brs.2018.04.011

The motor and sensory areas had the highest common optimal angle in most of the subjects. The occipital area also presented a high rate of common angle.

We next investigated the relationship between the optimal current direction and the motor cortical anatomy (Fig. 6A) as TMS can stimulate the hand motor area with a lower threshold and can target specific muscles if it induces a posterior-anterior directed electrical current (30). The computed optimal angle (Fig. 6-B1) and the angle normal to the sulcus wall (Fig. 6-B2) had a coefficient of determination R^2 = 0.8374 (Fig. 6C) for one subject. The standard deviation of the optimal angle is also shown in Fig. 6C (average of the standard deviation was 15.0˚) obtained from all possible angles between $0.9E_{\max}$ and $E_{\max}$. The averaged R^2 was 0.9114 for all subjects (95% confidence interval: 0.8974–0.9235).

Average Coil Shift

The optimal coil position does not necessarily correspond precisely to the nearest scalp point to the target cortical area (Fig. 7). In some cortical areas, we observed that the distances from the optimal scalp position for TMS to the scalp position nearest to the underlying cortex are within a 5-mm shift (e.g., premotor cortex and primary motor cortex). The mean position shift in the cortical surface was 5.5 ± 1.6 mm. The coil position shift and the cortex-scalp distance had a coefficient of determination R^2 = 0.4564, $p < 0.001$, in which larger cortex-scalp distances were related to larger coil shifts.

Comparison of Cortical Distribution Maps

We compared the $\overline{E}_{\max}$ values (Fig. 3-A1) among different cortical areas (Fig. 8A). A one-way ANOVA test (F (4, 21422) = 1277.8, $P < 0.001$), followed by a Bonferroni post hoc test, showed significant differences among all the regions in Fig. 8-B1. We also performed group comparisons of the maximum percentage of subjects with a common optimal angle (F(4, 20861) = 307.64, $P <$ 0.001, Fig 8-B2) and L_{shift} (F(4, 21422) = 397.74, $P < 0.001$, Fig. 8-B3). The difference in the number of subjects was statistically significant among the regions, except between frontal and

© 2018. This manuscript version is made available under the CC-BY-NC-ND 4.0 license
http://creativecommons.org/licenses/by-nc-nd/4.0/
Post-Print Version
https://doi.org/10.1016/j.brs.2018.04.011

parietal, while the distance shift was statistically significantly different among all the regions, except motor-sensory and occipital cortices. These results confirmed that: a) higher electric field strength was induced consistently in the motor and sensory areas, and b) the coil orientation map show that the most common optimal coil orientation was present at the motor and sensory areas.

Uncertainty factors

The number of stimulation positions, and its rotation angle resolution, together with tissue conductivity are uncertain factors in this study. To confirm their effect on the electric field distribution and optimal angle, a different number of stimulation positions (49×49 and 24×24) and angle steps (15˚ and 5˚) were used. Additionally, two sets of electrical conductivity were compared (current and one representative study, Table 1). As shown in Fig. 9 and Table 2, there was no noticeable difference in the electric field, and there was an acceptable difference in the optimal angle within the variability of the angle computation (Fig. 6).

Discussion

There is a large body of evidence that motor representation in the primary motor cortex has an optimal coil rotation angle (i.e., direction of the induced current), which depends on individual neuroanatomy (31–34). However, the selection of the most effective TMS coil configuration is not simple owing to the non-uniform current flow in the brain, and there are no described, measurable, biomarkers for cortical areas other than the motor cortex. Our computational study identified, for the first time, the optimal coil configuration (orientation/position) to induce maximal electric field strength across many subjects.

Atlas maps

The atlas of the electric field strength distribution (Fig. 3-A1) showed that the electric field was higher at the gyral crown than in the wall and this is in agreement with previous studies indicating that stimulation is likely to occur close to the gyral crown (13,19,35,36). The induced

© 2018. This manuscript version is made available under the CC-BY-NC-ND 4.0 license
http://creativecommons.org/licenses/by-nc-nd/4.0/
Post-Print Version
https://doi.org/10.1016/j.brs.2018.04.011

electric field strength significantly differed between cortical regions (Fig. 8-B1). The maximum strengths were induced consistently at the primary motor cortex, in particular, the hand motor area, whereas less current was induced in the occipital region. This result is supported by a previous finding that rTMS intensity for long-lasting effects on visual evoked potentials (37) was higher than the resting motor threshold for M1 (38). The optimal electric field strength can be predicted to a certain extent from the cortex-scalp distance ($R^2 = 0.7985$) as shown in Fig. 4A and 4B (26). From a practical point of view, the cortex-scalp distance can be used as a predictor of induced electric-field distribution. However, the distance alone is neither able to predict field distribution accurately nor provide information about the optimal coil orientation.

Fig. 5-A1 shows the optimal coil orientation for the study group. The optimal induced current direction was approximately perpendicular to the gyrus in all cortical areas. This is consistent with experimental results in the hand motor area (10,27–29). The best current direction for Broca's area in our atlas agrees with the experimental results of language mapping using anterior-posterior or medial-lateral directed currents (38). For the motor and sensory areas, most of the subjects had a common optimal angle (Fig. 5-A2 and Fig. 8-B2) (10). One possible explanation for the discrepancy between the regions may be that the central sulcus is approximately in the same direction in all individuals. In contrast, other regions have complicated, variable folding patterns between individuals.

Coil localization is another important factor for TMS. One of our aims was to investigate how far the optimal scalp coil position deviates from the scalp point nearest to the target cortical area. Fig. 7 and Fig. 8-B3 show that this distance was smallest at the motor, sensory, and occipital areas (< 5 mm). This indicates that, anatomical information could be used to estimate the optimal coil position for these areas. Although not presented in this work, the direction of the coil shift could be useful for atlas-based targeting for regions with largest distance shifts (i.e., parietal and temporal lobes). The best optimal position may require personalized coil localization when high accuracy is needed.

© 2018. This manuscript version is made available under the CC-BY-NC-ND 4.0 license
http://creativecommons.org/licenses/by-nc-nd/4.0/
Post-Print Version
https://doi.org/10.1016/j.brs.2018.04.011

Universal or personalized method

The atlas maps can help to guide general TMS coil configuration to specific cortical areas in a group of subjects. For instance, this atlas suggests that a common optimal angle applicable to most subjects is more feasible at the motor or sensory areas. For other regions, a universal coil angle was not available (Fig. 5-A2). For such areas, personalized optimization of the coil orientation and position would be preferable (39) in which the induced current direction (coil orientation) is perpendicular to the sulcus wall (32,33). However, it has not been computed how the spatial distribution of the electrical fields in the stimulated cortex affects the optimal coil orientation and whether it agrees with the current direction normal to the sulcus wall. The present computational study showed that the optimal coil angle follows the anatomical shape of the hand motor area (R^2 = 0.9114, n = 18), as shown in Fig. 6C. This evidence supports the use of the anatomical information offered by MRI to maximize TMS mapping.

Limitations

In the present study, we investigated many more stimulation scenarios than those previously reported (5,9,40), but it is difficult to say how many subjects, which angle resolution, and stimulation grid resolution are needed for certainty. We confirmed that the results are robust with the parameters selected, as shown in the subsection 'Uncertainty factor of Results.' The current study focused solely on the electric field strength without consideration of the target neurons and its orientation (13,19,35,36). Electric field strength is not the only factor affecting neural activation. The final effects of TMS would also depend on stimulation frequency and geometric configuration of the coil, as well as physiological (e.g., sex and age) and cognitive states (41).

Conclusion

This study developed an atlas of optimal TMS electric fields, coil orientations/positions for all cortical regions. To derive the atlas, 518,616 different scenarios were challenged. The electric

© 2018. This manuscript version is made available under the CC-BY-NC-ND 4.0 license
http://creativecommons.org/licenses/by-nc-nd/4.0/
Post-Print Version
https://doi.org/10.1016/j.brs.2018.04.011

field map shows that significant higher electric field strength is consistently induced in the motor and sensory areas. The coil orientation map also shows that the most common optimal coil orientation is seen in the motor and sensory areas. The optimal coil position for motor and sensory areas can be estimated from individual anatomical information. The maps can be used as an initial guide for selecting the TMS parameters when a neuro-navigation system is not available, especially for a region other than the motor cortex. The present computational study confirms that the optimal coil angle follows the anatomical shape of the hand motor area. It supports that the personalized optimal coil orientation should be used for estimating the most effective stimulation. Future studies are needed to elaborate the precise correlation between the induced current parameters and neural anatomy.

© 2018. This manuscript version is made available under the CC-BY-NC-ND 4.0 license
http://creativecommons.org/licenses/by-nc-nd/4.0/
Post-Print Version
https://doi.org/10.1016/j.brs.2018.04.011

Declarations of interest: none

Acknowledgements

This work was supported in part by KAKENHI 17H05293.

© 2018. This manuscript version is made available under the CC-BY-NC-ND 4.0 license
http://creativecommons.org/licenses/by-nc-nd/4.0/
Post-Print Version
https://doi.org/10.1016/j.brs.2018.04.011

References

1. Barker AT, Jalinous R, Freeston IL. Non-invasive magnetic stimulation of human motor cortex. Lancet (London, England). 1985 May 11;1(8437):1106–7.
2. Rademacher J, Caviness VS, Steinmetz H, Galaburda AM. Topographical variation of the human primary cortices: implications for neuroimaging, brain mapping, and neurobiology. Cereb Cortex. 1993;3(4):313–29.
3. Miranda PC, Correia L, Salvador R, Basser PJ. Tissue heterogeneity as a mechanism for localized neural stimulation by applied electric fields. Phys Med Biol. IOP Publishing; 2007 Sep 21;52(18):5603–17.
4. Opitz A, Windhoff M, Heidemann RM, Turner R, Thielscher A. How the brain tissue shapes the electric field induced by transcranial magnetic stimulation. Neuroimage. Elsevier Inc.; 2011;58(3):849–59.
5. Janssen AM, Oostendorp TF, Stegeman DF. The effect of local anatomy on the electric field induced by TMS: evaluation at 14 different target sites. Med Biol Eng Comput. Springer Berlin Heidelberg; 2014 Oct 28;52(10):873–83.
6. Tachas NJ, Efthimiadis KG, Samaras T. The Effect of Coil Modeling on the Predicted Induced Electric Field Distribution During TMS. IEEE Trans Magn. 2013 Mar;49(3):1096–100.
7. Iwahashi M, Gomez-Tames J, Laakso I, Hirata A. Evaluation method for *in situ* electric field in standardized human brain for different transcranial magnetic stimulation coils. Phys Med Biol. IOP Publishing; 2017 Mar 21;62(6):2224–38.
8. Rossi S, Hallett M, Rossini PM, Pascual-Leone A, Safety of TMS Consensus Group TS of TC. Safety, ethical considerations, and application guidelines for the use of transcranial magnetic stimulation in clinical practice and research. Clin Neurophysiol. NIH Public Access; 2009 Dec;120(12):2008–39.
9. Laakso I, Hirata A, Ugawa Y. Effects of coil orientation on the electric field induced by TMS over the hand motor area. Phys Med Biol. 2014 Jan 6;59(1):203–18.
10. Richter L, Neumann G, Oung S, Schweikard A, Trillenberg P. Optimal coil orientation for transcranial magnetic stimulation. PLoS One. Public Library of Science; 2013;8(4):e60358.
11. Nummenmaa A, McNab JA, Savadjiev P, Okada Y, Hämäläinen MS, Wang R, et al. Targeting of White Matter Tracts with Transcranial Magnetic Stimulation. Brain Stimul. 2014 Jan;7(1):80–4.
12. Sakai K, Ugawa Y, Terao Y, Hanajima R, Furubayashi T, Kanazawa I. Preferential activation of different I waves by transcranial magnetic stimulation with a figure-of-eight-shaped coil. Exp Brain Res. Springer-Verlag; 1997 Jan;113(1):24–32.
13. Bungert A, Antunes A, Espenhahn S, Thielscher A. Where does TMS Stimulate the Motor Cortex? Combining Electrophysiological Measurements and Realistic Field Estimates to Reveal the Affected Cortex Position. Cereb Cortex. 2016 Sep 24;120:141–57.
14. Dale AM, Fischl B, Sereno MI. Cortical Surface-Based Analysis. Neuroimage. 1999 Feb;9(2):179–94.
15. Fischl B. FreeSurfer. Neuroimage. 2012 Aug 15;62(2):774–81.
16. Laakso I, Tanaka S, Koyama S, De Santis V, Hirata A. Inter-subject Variability in Electric Fields of Motor Cortical tDCS. Brain Stimul. 2015;8(5):906–13.
17. Gabriel S, Lau RW, Gabriel C. The dielectric properties of biological tissues: III. Parametric models for the dielectric spectrum of tissues. Phys Med Biol. IOP Publishing; 1996 Nov 1;41(11):2271–93.
18. Nieminen JO, Koponen LM, Ilmoniemi RJ. Experimental Characterization of the Electric Field Distribution Induced by TMS Devices. Brain Stimul. 2015;8(3):582–9.
19. Opitz A, Zafar N, Bockermann V, Rohde V, Paulus W. Validating computationally predicted

© 2018. This manuscript version is made available under the CC-BY-NC-ND 4.0 license
http://creativecommons.org/licenses/by-nc-nd/4.0/
Post-Print Version
https://doi.org/10.1016/j.brs.2018.04.011

TMS stimulation areas using direct electrical stimulation in patients with brain tumors near precentral regions. NeuroImage Clin. 2014;4:500–7.

20. Thielscher A, Opitz A, Windhoff M. Impact of the gyral geometry on the electric field induced by transcranial magnetic stimulation. Neuroimage. 2011 Jan 1;54(1):234–43.

21. Janssen A, Oostendorp T. The coil orientation dependency of the electric field induced by TMS for M1 and other brain areas. J Neuroeng Rehabil. 2015;12(1):47.

22. Laakso I, Hirata A. Fast multigrid-based computation of the induced electric field for transcranial magnetic stimulation. Phys Med Biol. 2012;57(23):7753–65.

23. Silver NC, Dunlap WP. Averaging correlation coefficients: Should Fisher's z transformation be used? J Appl Psychol. 1987;72(1):146–8.

24. Fonov V, Evans AC, Botteron K, Almli CR, McKinstry RC, Collins DL, et al. Unbiased average age-appropriate atlases for pediatric studies. Neuroimage. NIH Public Access; 2011 Jan 1;54(1):313–27.

25. Fonov V, Evans A, McKinstry R, Almli C. Unbiased nonlinear average age-appropriate brain templates from birth to adulthood. NeuroImage . 2009;47.

26. Deng Z-D, Lisanby SH, Peterchev A V. Electric field depth–focality tradeoff in transcranial magnetic stimulation: Simulation comparison of 50 coil designs. Brain Stimul. 2013;6(1):1–13.

27. Fox PT, Narayana S, Tandon N, Sandoval H, Fox SP, Kochunov P, et al. Column-based model of electric field excitation of cerebral cortex. Hum Brain Mapp. 2004 May;22(1):1–14.

28. Mills KR, Boniface SJ, Schubert M. Magnetic brain stimulation with a double coil: the importance of coil orientation. Electroencephalogr Clin Neurophysiol Potentials Sect. 1992 Feb;85(1):17–21.

29. Brasil-Neto JP, Cohen LG, Panizza M, Nilsson J, Roth BJ, Hallett M. Optimal focal transcranial magnetic activation of the human motor cortex: effects of coil orientation, shape of the induced current pulse, and stimulus intensity. J Clin Neurophysiol. 1992 Jan;9(1):132–6.

30. Di Lazzaro V, Restuccia D, Oliviero A, Profice P, Ferrara L, Insola A, et al. Effects of voluntary contraction on descending volleys evoked by transcranial stimulation in conscious humans. J Physiol. Wiley-Blackwell; 1998 Apr 15;508 (Pt 2)(Pt 2):625–33.

31. Stephani C, Paulus W, Sommer M. The effect of current flow direction on motor hot spot allocation by transcranial magnetic stimulation. Physiol Rep. Wiley-Blackwell; 2016 Jan;4(1).

32. Bashir S, Perez JM, Horvath JC, Pascual-Leone A. Differentiation of Motor Cortical Representation of Hand Muscles by Navigated Mapping of Optimal TMS Current Directions in Healthy Subjects. J Clin Neurophysiol. 2013 Aug;30(4):390–5.

33. Raffin E, Pellegrino G, Di Lazzaro V, Thielscher A, Siebner HR. Bringing transcranial mapping into shape: Sulcus-aligned mapping captures motor somatotopy in human primary motor hand area. Neuroimage. 2015 Oct 15;120:164–75.

34. Guggisberg AG, Dubach P, Hess CW, Wüthrich C, Mathis J. Motor evoked potentials from masseter muscle induced by transcranial magnetic stimulation of the pyramidal tract: the importance of coil orientation. Clin Neurophysiol. 2001 Dec;112(12):2312–9.

35. Laakso I, Murakami T, Hirata A, Ugawa Y. Experiments and modelling pinpoint the cortical activation site of TMS. Brain Stimul. Elsevier; 2017 Mar;10(2):460–1.

36. Aonuma S, Gomez-Tames J, Laakso I, Hirata A, Takakura T, Tamura M, et al. A high-resolution computational localization method for transcranial magnetic stimulation mapping. Neuroimage. 2018;172:85–93.

37. Bohotin V, Fumal A, Vandenheede M, Gérard P, Bohotin C, Maertens de Noordhout A, et al. Effects of repetitive transcranial magnetic stimulation on visual evoked potentials in migraine. Brain. 2002 Apr;125(Pt 4):912–22.

38. Sollmann N, Ille S, Obermueller T, Negwer C, Ringel F, Meyer B, et al. The impact of repetitive navigated transcranial magnetic stimulation coil positioning and stimulation parameters on human language function. Eur J Med Res. BioMed Central; 2015 Apr 1;20(1):47.

© 2018. This manuscript version is made available under the CC-BY-NC-ND 4.0 license
http://creativecommons.org/licenses/by-nc-nd/4.0/
Post-Print Version
https://doi.org/10.1016/j.brs.2018.04.011

39. Meincke J, Hewitt M, Batsikadze G, Liebetanz D. Automated TMS hotspot-hunting using a closed loop threshold-based algorithm. Neuroimage. 2016 Jan 1;124(Pt A):509–17.

40. Opitz A, Fox MD, Craddock RC, Colcombe S, Milham MP. An integrated framework for targeting functional networks via transcranial magnetic stimulation. Neuroimage. 2016 Feb 15;127:86–96.

41. Miniussi C, Harris JA, Ruzzoli. M. Modelling non-invasive brain stimulation in cognitive neuroscience. Neurosci Biobehav Rev. Pergamon; 2013 Sep 1;37(8):1702–12.

© 2018. This manuscript version is made available under the CC-BY-NC-ND 4.0 license
http://creativecommons.org/licenses/by-nc-nd/4.0/
Post-Print Version
https://doi.org/10.1016/j.brs.2018.04.011

Table and Figure Legends

Table 1 Two sets of tissue conductivity values are used for the head model. Set A corresponds to the values reported in (17) and Set B to typical values in TMS computational models (19–21)

Tissues	Conductivity [S/m]	
	Set A	Set B
Blood	0.7	0.7
Bone (Cancellous)	0.08	0.025
Bone (Cortical)	0.02	0.007
Brain (cerebellum)	0.15	0.276
Brain (gray matter)	0.13	0.276
Brain (white matter)	0.08	0.126
Cerebrospinal fluid	2.0	1.654
Dura	0.5	0.5
Fat	0.04	0.04
Muscle	0.36	0.400
Mucous membrane	0.07	0.07
Skin	0.00045	0.456
Vitreous humor	1.5	1.500

© 2018. This manuscript version is made available under the CC-BY-NC-ND 4.0 license
http://creativecommons.org/licenses/by-nc-nd/4.0/
Post-Print Version
https://doi.org/10.1016/j.brs.2018.04.011

Table 2. Effect of different resolution of computations parameters

	Error Electric Field Strength (%)	Error Optimal Angle [deg]
Position Grid	0.48±0.58	4.63±9.48
Angle	0.51±0.58	6.1±9.05
Conductivity	4.08±3.36	12.5±17.8

© 2018. This manuscript version is made available under the CC-BY-NC-ND 4.0 license
http://creativecommons.org/licenses/by-nc-nd/4.0/
Post-Print Version
https://doi.org/10.1016/j.brs.2018.04.011

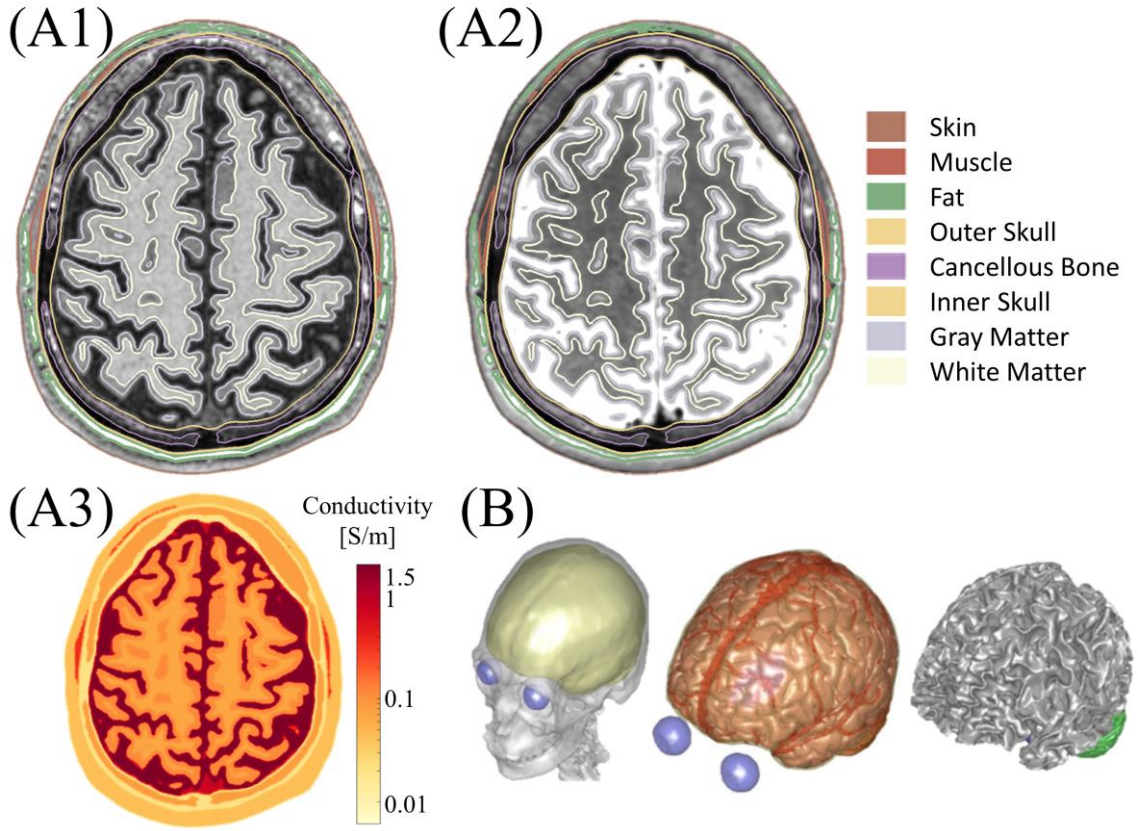

Fig. 1. Volume conductor model constructed from an MRI. (A1-A2) Superior views of the axial slices of the T1- and T2-weighted MRI with the boundary of some tissues visible. (A3) Electrical conductivity of final segmented tissues. (B) Surface of some segmented tissues: outer and inner skull surfaces, grey matter, and white matter. The surfaces obtained were used to voxelize the segmented model. Cerebrospinal fluid is the region between inner skull and grey matter.

© 2018. This manuscript version is made available under the CC-BY-NC-ND 4.0 license
http://creativecommons.org/licenses/by-nc-nd/4.0/
Post-Print Version
https://doi.org/10.1016/j.brs.2018.04.011

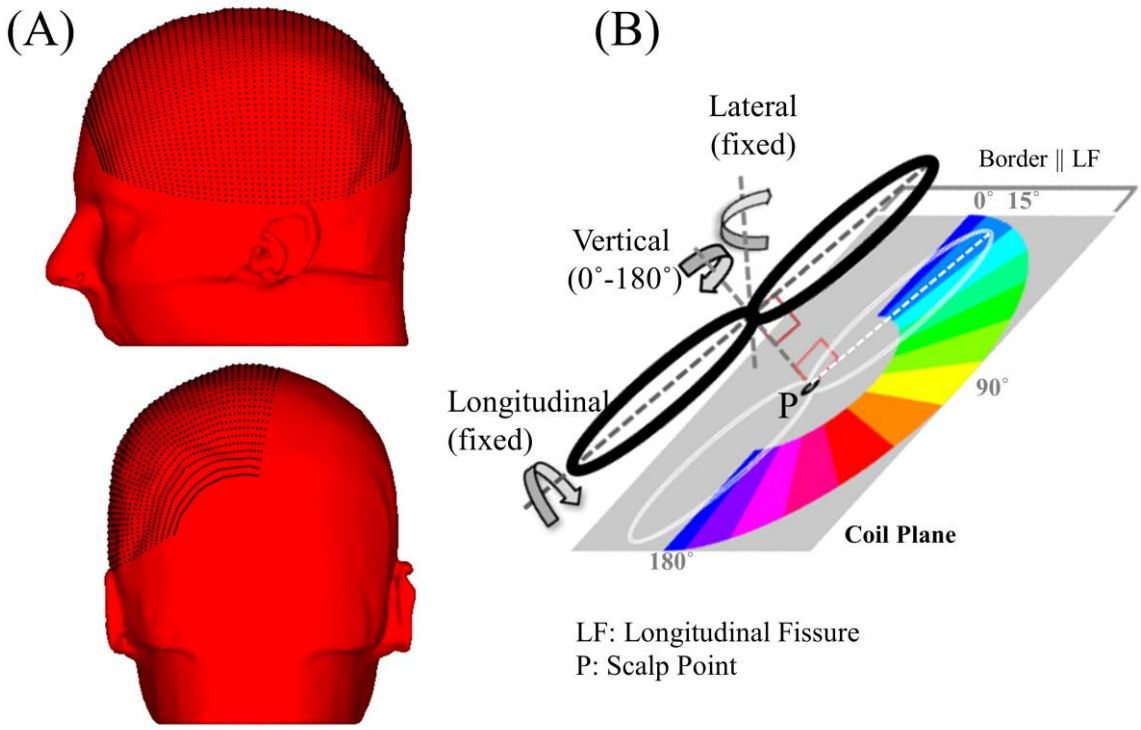

Fig. 2. The TMS coil was placed over 2401 points of the grid and oriented at twelve different vertical orientations for each subject (n = 18). (A) Lateral view and coronal view. (B) The coil orientation was presented for a point P in the scalp surface. In this case, the coil was rotated 15˚.

© 2018. This manuscript version is made available under the CC-BY-NC-ND 4.0 license
http://creativecommons.org/licenses/by-nc-nd/4.0/
Post-Print Version
https://doi.org/10.1016/j.brs.2018.04.011

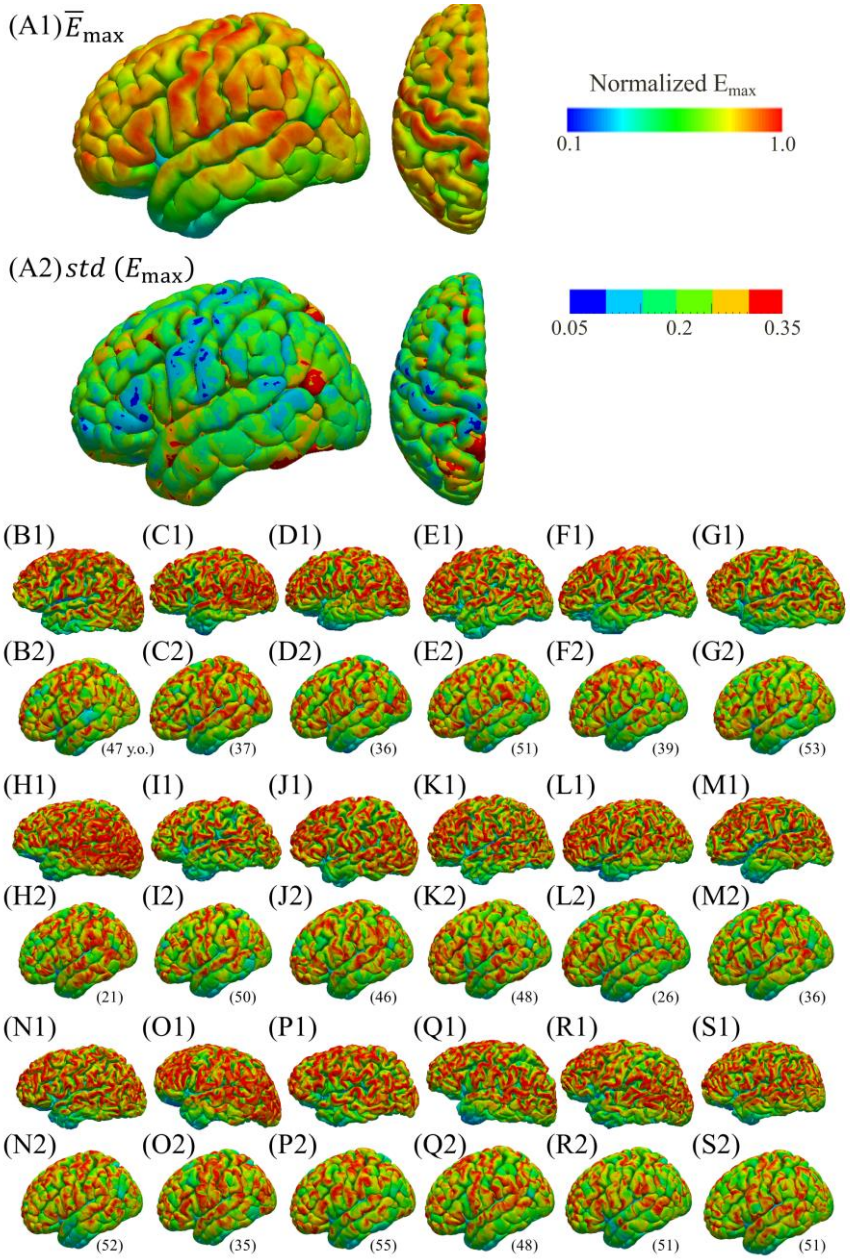

Fig. 3. Electric field distribution. (A1-A2) Average and relative standard deviation of the electric field for a group of subjects in the standard brain space (n = 18). (B-S) Individualized electric fields in (1) original cortical surface and (2) standard brain space. The subjects' age is shown in parenthesis. A 3D version is included as supplementary material.

© 2018. This manuscript version is made available under the CC-BY-NC-ND 4.0 license
http://creativecommons.org/licenses/by-nc-nd/4.0/
Post-Print Version
https://doi.org/10.1016/j.brs.2018.04.011

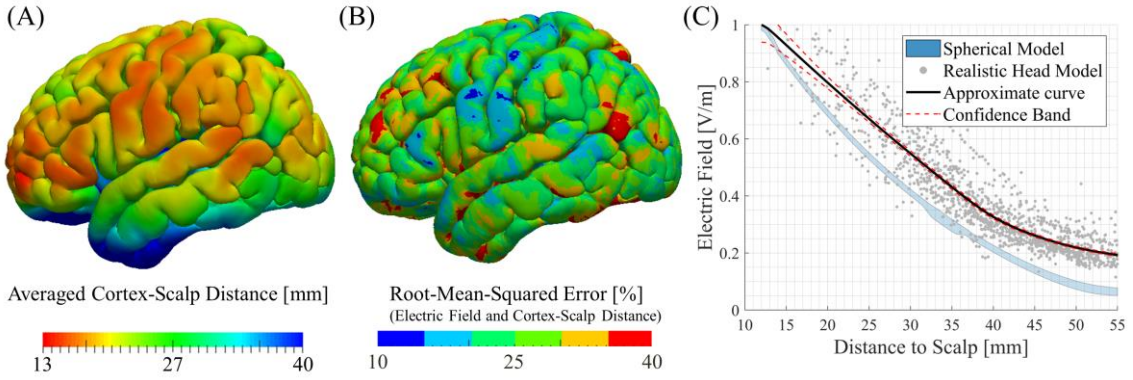

Fig. 4. (A) Averaged cortex-scalp distance (n = 18). (B) Root-mean-squared error (percentage of magnitude) between the electric field strength and cortex-scalp distance at each cortical point of eighteen subjects registered in the standard brain space (n = 18). (C) Relationship of the induced electric field and the distance from the scalp (n = 18). The electric field values in the head models were selected randomly along the inward normal at different scalp points. The electric field using the spherical model corresponds to the minimum and maximum results for radii between 9.1 cm to 9.7 cm. Nonparametric fitting was used to extract the fitted data and paired bootstrap to obtain the confidence band.

© 2018. This manuscript version is made available under the CC-BY-NC-ND 4.0 license
http://creativecommons.org/licenses/by-nc-nd/4.0/
Post-Print Version
https://doi.org/10.1016/j.brs.2018.04.011

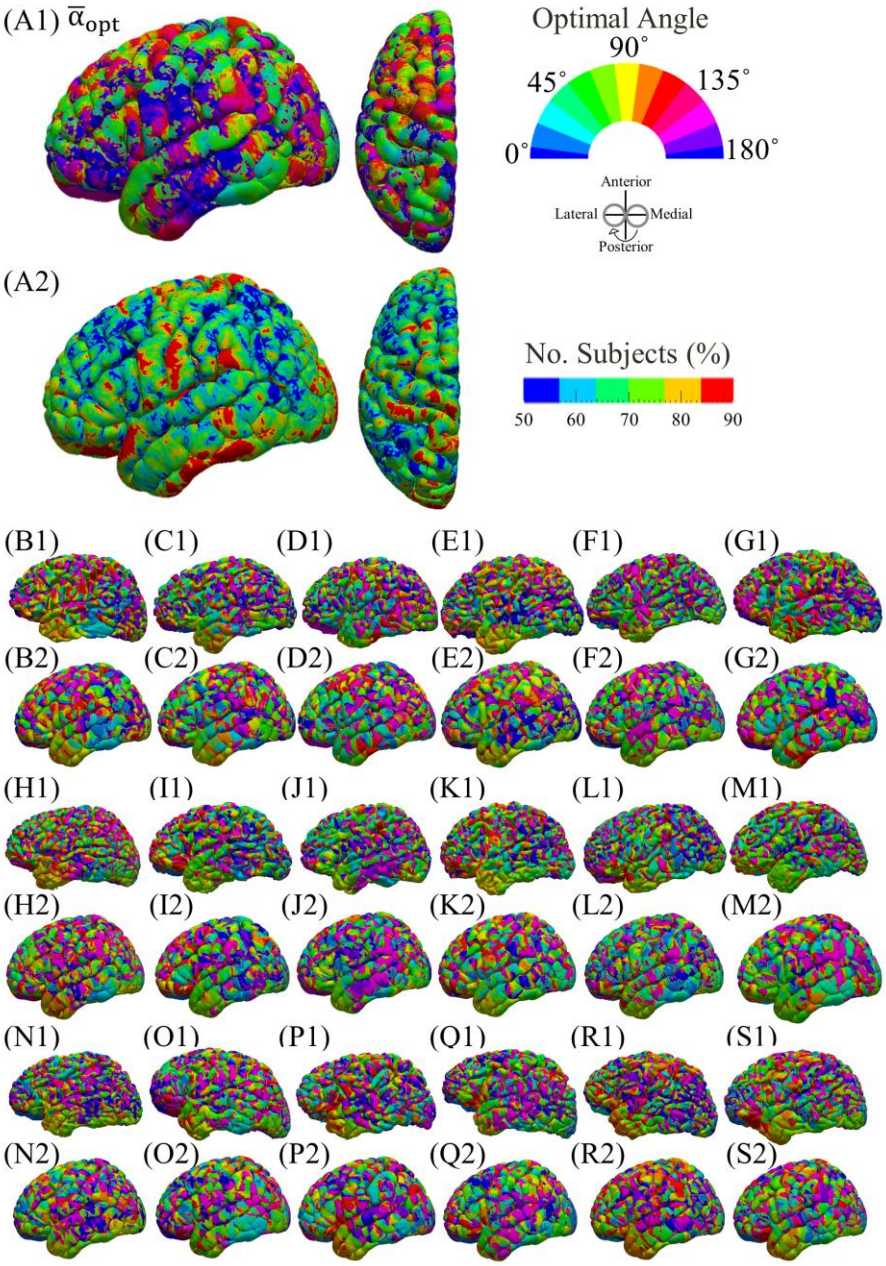

Fig. 5. Optimal TMS coil orientation. (A1) Most common optimal coil orientation for a group of subjects in standard brain space (n = 18). (A2) Maximum number of subjects with common optimal angle in A1. (B–S) Individualized optimal coil orientation in the (1) original cortical surface and (2) standard brain space. The angle rotation is presented in Fig. 2. A 3D version is included as supplementary material.

© 2018. This manuscript version is made available under the CC-BY-NC-ND 4.0 license
http://creativecommons.org/licenses/by-nc-nd/4.0/
Post-Print Version
https://doi.org/10.1016/j.brs.2018.04.011

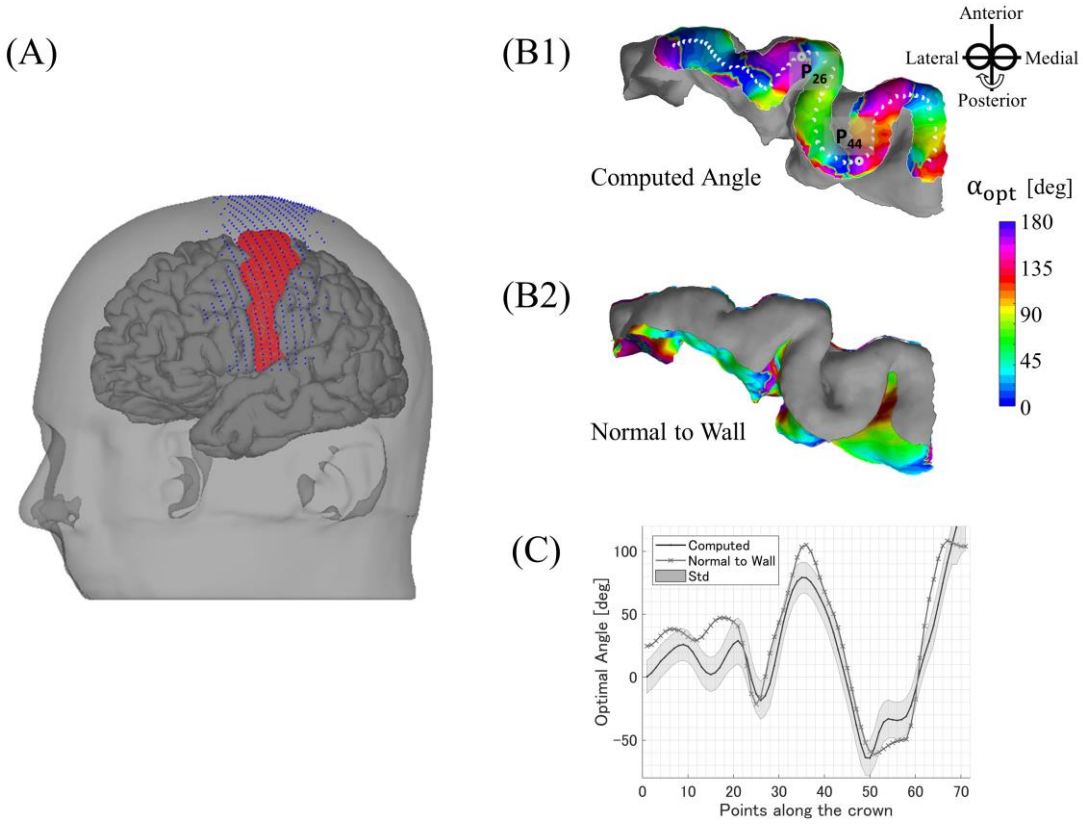

Fig. 6. Relationship between computed optimal angle and normal vector to wall. (A) Stimulation positions for motor area. (B1) Optimal angle and selected sample points. (B2) Normal angle to the wall. (C) Angle comparison. The angle was determined as the median of each sample point and its 10 nearest points. Standard deviation of the optimal angle is for angles obtained for $0.9E_{\max}$ or larger.

© 2018. This manuscript version is made available under the CC-BY-NC-ND 4.0 license
http://creativecommons.org/licenses/by-nc-nd/4.0/
Post-Print Version
https://doi.org/10.1016/j.brs.2018.04.011

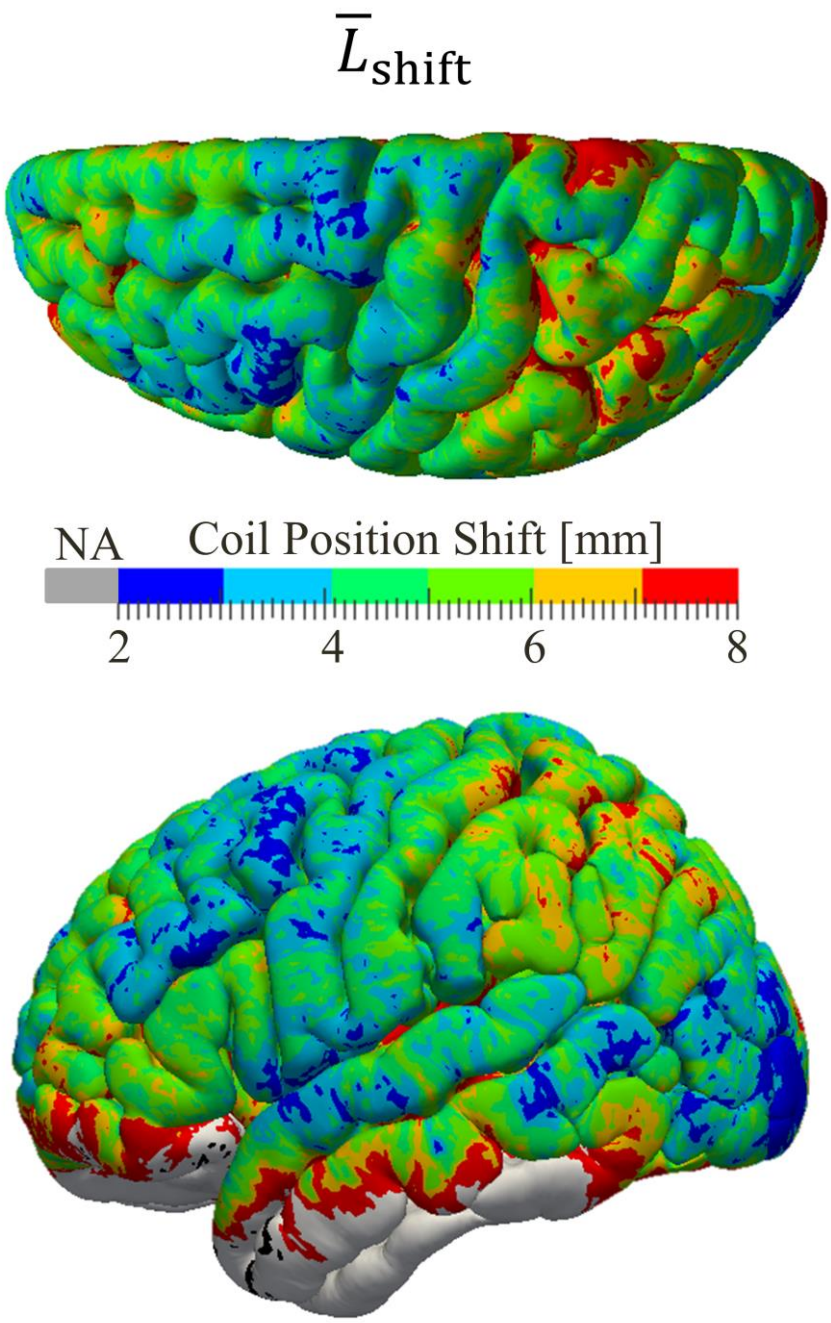

Fig. 7. Distance shift between the optimal coil position and nearest scalp position to each cortical point (n = 18). A 3D version is included as supplementary material. NA: not available.

© 2018. This manuscript version is made available under the CC-BY-NC-ND 4.0 license
http://creativecommons.org/licenses/by-nc-nd/4.0/
Post-Print Version
https://doi.org/10.1016/j.brs.2018.04.011

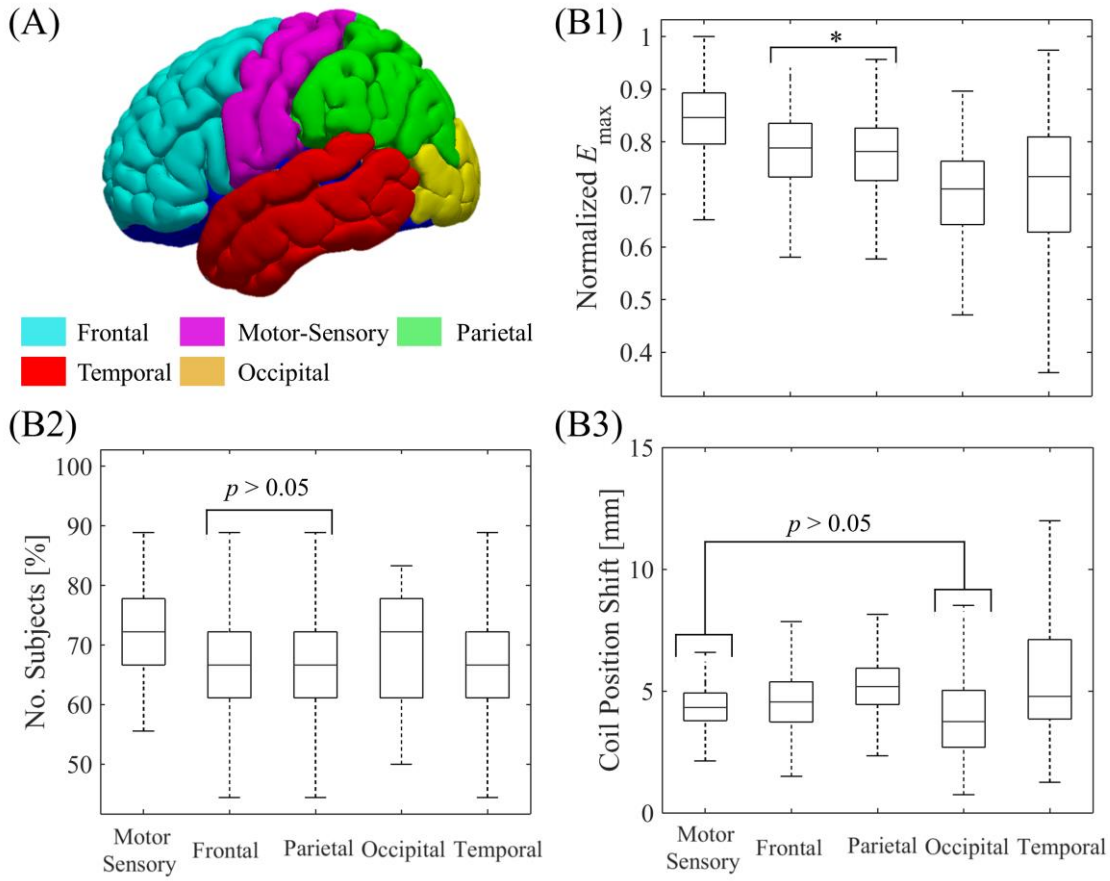

Fig. 8 Comparisons of cortical distributions maps. (A) The cortex is divided into five regions. (B1) Maximum electric field strength. (B2) Maximum percentage of subjects with common coil orientation. (B3) Distance shift of the coil position in the scalp. A one-way ANOVA, followed by Bonferroni-corrected post hoc t-tests, showed significant differences between all regions except frontal and parietal (B2) and motor-sensory and occipital (B3). *$p < 0.01$ and interaction no explicitly indicated corresponds to $p < 0.001$.

© 2018. This manuscript version is made available under the CC-BY-NC-ND 4.0 license
http://creativecommons.org/licenses/by-nc-nd/4.0/
Post-Print Version
https://doi.org/10.1016/j.brs.2018.04.011

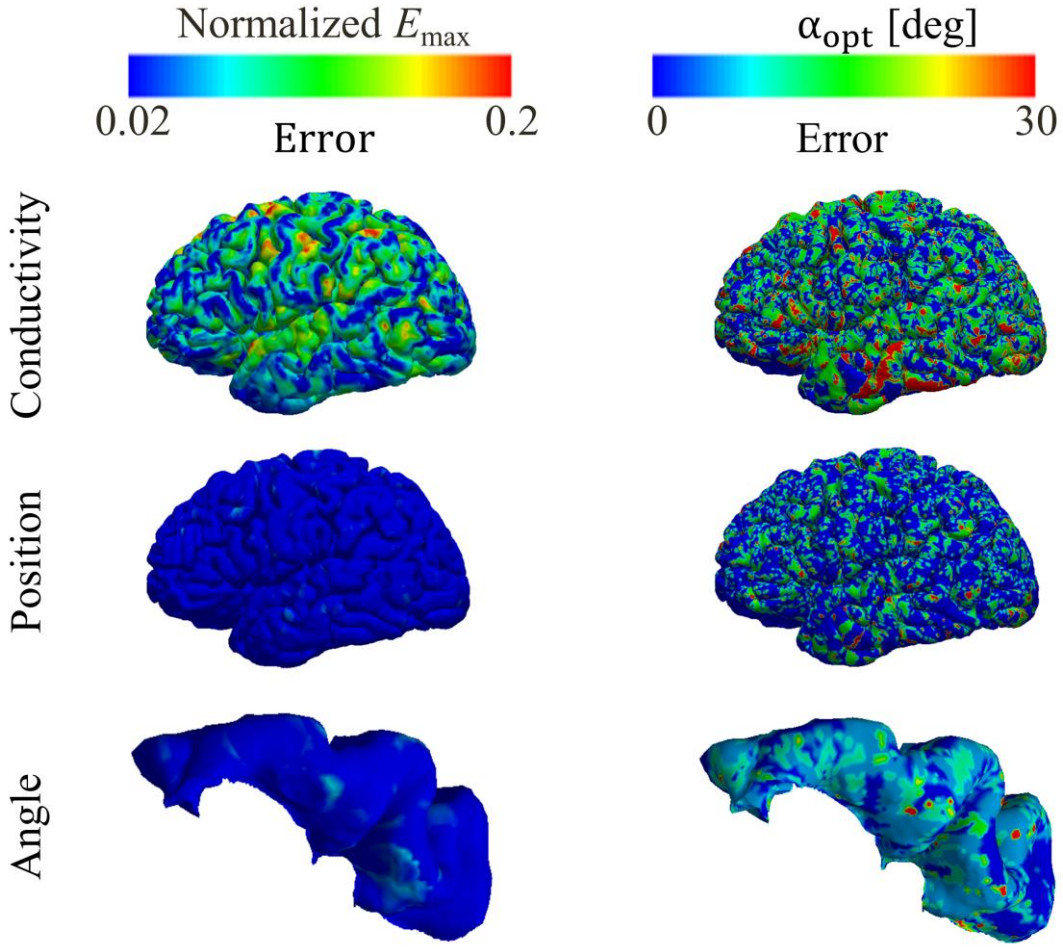

Fig. 9 Electric field strength and optimal angle variation for two different sets of conductivity, grid resolution for coil positions (24×24 and 49×49 positions), and angle resolution (15˚ and 5˚)